

Selective Small-Molecule Activator of Patient-Derived GPX4 Variant

Hengrui Liu, Farhad Forouhar, Russell Saneto, and Brent R. Stockwell*

Cite This: <https://doi.org/10.1021/acschembio.5c00158>

Read Online

ACCESS |



Metrics & More

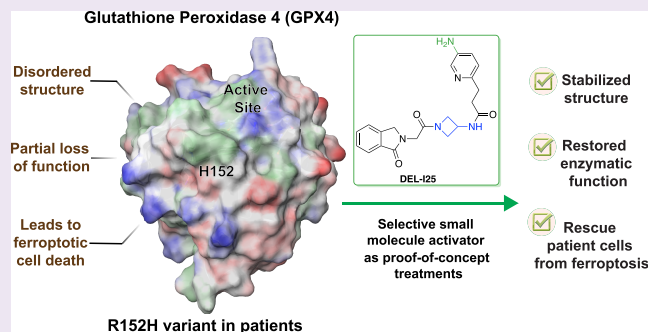


Article Recommendations



Supporting Information

ABSTRACT: Glutathione peroxidase 4 (GPX4) is distinguished from other members of the GPX family as being the enzyme capable of reducing phospholipid hydroperoxides within cellular membranes and therefore protecting cells from ferroptosis, a form of iron-driven cell death involving lipid peroxidation. We previously identified a homozygous point mutation in the *GPX4* gene, resulting in an R152H coding mutation and a substantial loss of GPX4 enzymatic activity, in patients with Sedaghatian-type spondylometaphyseal dysplasia (SSMD), an ultrarare progressive disorder. To explore whether selective binding and correction of the loss of enzyme activity observed with this variant is possible, we screened 2.8 billion compounds in a DNA-encoded chemical library and identified compounds with remarkably selective binding affinities with the R152H variant (GPX4^{R152H}) over wild-type (GPX4^{WT}). Our structural optimization of these compounds led to the identification of analogues with improved potency for R152H GPX4. The most promising compounds selectively restored the enzyme activity of GPX4^{R152H} and specifically increased the viability of fibroblast and lymphoblast cells developed from an SSMD patient with the homozygous R152H variation but not control cells from a healthy parent or HEK293T cells undergoing ferroptosis induced by a wild-type GPX4 inhibitor. This approach represents a low-cost, high-throughput, and generalizable approach to identify targeted small-molecule therapeutics for missense variants, which features the potential to be broadly applied to diseases that bear point mutations on crucial proteins, including cancers.



INTRODUCTION

Glutathione peroxidase 4 (GPX4), one of the 25 selenocysteine-containing proteins encoded in the human genome, is capable of reducing lipid hydroperoxides to nontoxic lipid alcohols, at the expense of reduced glutathione or other thiols.¹ Different from the other seven members of glutathione peroxidase family (GPXs), GPX4 is distinguished for its ability to reduce a broad spectrum of peroxide substrates, including hydrogen peroxide, organic hydroperoxides, and lipid (cholesterol, phospholipid) peroxides.² Peroxidation of phospholipids, which compose the lipid bilayers that make up cellular membranes, is a key driver of ferroptosis, an iron-dependent form of nonapoptotic cell death.³ This unique function underlies the essential role of GPX4 to protect cells from ferroptosis.⁴

We previously identified a variant in the *GPX4* gene, c.523 G > A (based on NCBI Reference Sequence NM_001367832.1), which resulted in an R152H coding variant found to be homozygous in three patients with Sedaghatian-type spondylometaphyseal dysplasia (SSMD), an ultrarare progressive disorder.⁵ These patients were characterized by metaphyseal chondrodysplasia with mild limb shortening, platyspondyly, and cardiorespiratory defects, in addition to auditory neuropathy, optic nerve hypoplasia, hypotonia, and severe motor delays. We examined the molecular impact of the R152H variant and found that it profoundly disrupted the structure of a critical loop (P124–N137, which we termed the G-loop, as it is glycine-rich

and substantially impaired the enzymatic activity of GPX4. At the cellular level, no significant change in the expressional level or subcellular localization of GPX4 was observed when patient fibroblast cells were compared with control cells from a healthy parent.

We aimed to develop a precision medicine for SSMD patients with the R152H variant. Considering that a conformational change in a critical loop is the exclusive structural difference between GPX4^{WT} and GPX4^{R152H}, we hypothesized that GPX4^{R152H}-specific small-molecule binders might interact with and stabilize this critical loop, restore GPX4 enzymatic activity to the normal level, and therefore alleviate the pathological features caused by impaired GPX4^{R152H} activity.

To search for variant-specific binders, we took advantage of a DNA-encoded chemical library (DEL) that enables the screening of billions of compounds in a single experiment. This advantage of DEL is achieved by large-scale creation of DNA-labeled compounds using combinatorial chemistry, so that a minimal amount of individual library molecules is required

Received: March 1, 2025

Revised: April 17, 2025

Accepted: April 23, 2025

in each screen and hits can be easily decoded by reading DNA barcodes.⁶ Here, we report using a DELopen library in small-molecule discovery, and we envision that the broadened use of DEL technology may expedite precision medicines for rare diseases.

We sought to aid SSMD patients with the R152H variant with precision treatment by activating this deficient enzyme. Additionally, GPX4 has been reported to be a promising therapeutic target for drug-resistant and metastatic cancers, based on the elevated dependency of these cancers on the GPX4 lipid peroxide repair pathway.^{7–9} We hypothesized that greater insight into the enzymatic mechanism of GPX4 might emerge from studying a patient-derived loss-of-function variant, providing guidance on how to modulate GPX4 activity more generally for therapeutic benefit.

Large-scale expression of selenocysteine-containing proteins such as GPX4 in recombinant systems is challenging due to inefficient selenocysteine-incorporation machinery; thus, the selenocysteine to cysteine (U to C, inserting a thiol group in place of the selenol group) mutant of GPX4 was used for structural studies, despite its lower enzymatic activity compared to the wild-type protein.^{10–13} Since recent structural studies on selenocysteine-containing GPX4 confirmed the relevance of the catalytic triad and other structural properties discovered in the context of the U to C mutant,^{14–17} we used a GPX4^{U46C} construct for in vitro screening and structural studies and simultaneously examined the selenocysteine-containing cytosolic GPX4 protein in human cells via enzymatic assays and cellular assays.

We identified screening hits that could selectively bind to GPX4^{R152H}, elevate its enzyme activity, and specifically increase the viability of fibroblast and lymphoblast cells derived from an SSMD patient with the R152H variant. Structural optimization of hit compounds led to the discovery of analogues with improved therapeutic potency for R152H GPX4. This study illustrates a general approach to identifying targeted small-molecule therapeutics for patients with missense mutations on crucial proteins.

RESULTS

Identification of R152H-Selective Binders from DNA-Encoded Chemical Library Screening. Aiming to identify GPX4^{R152H}-specific protein binders that can restore enzymatic activity toward the normal level and therefore alleviate pathological features, we screened 2.8 billion compounds in a DNA-encoded chemical library (DELopen by WuXi AppTec) using an affinity pull-down assay. We captured His-tagged GPX4 protein on Ni-NTA magnetic beads before incubation with a DELopen library (Supplementary Figure S1A). GPX4 beads or control empty beads were magnetically pulled down and extensively washed before being heated to 95 °C to release bound library molecules. Inclusion of both GPX4^{R152H} and GPX4^{WT} in the screen facilitated a search for variant-specific binders.

Four compounds (DEL-H through DEL-K, termed Group 3) emerged as top screening hits with enrichment for GPX4^{R152H} compared to both GPX4^{WT} and a negative control (Figure 1). We picked two compounds (DEL-A and DEL-B, termed Group 1) that selectively enriched for binding to GPX4^{WT}, and five compounds (DEL-C through DEL-G, termed Group 2) that enriched for binding to both GPX4^{WT} and GPX4^{R152H} (Supplementary Figure S1B) over background control. Group 1 and 2 serve as controls for R152H specificity in Group 3.

A

Screening Hits	Enrichment index on immobilized protein			Group	
	Negative control	GPX4 ^{WT} replicate #1	GPX4 ^{WT} replicate #2		GPX4 ^{R152H}
DEL -A	0.1	1109.7	881.9	0.1	Group 1: WT selective
DEL -B	0.1	1466.4	821.1	0.1	
DEL -C	0.1	1373.2	1024.4	1303.1	Group 2: pan-GPX4
DEL -D	0.1	1706.1	866.8	1172.8	
DEL -E	0.1	1248.3	971.8	999.0	
DEL -F	0.1	1683.8	705.1	1155.0	
DEL -G	0.1	1279.7	940.1	935.0	
DEL -H	0.1	0.1	0.1	462.6	Group 3: R152H selective
DEL -I	0.1	0.1	0.1	260.6	
DEL -J	0.1	0.1	0.1	275.0	
DEL -K	0.1	0.1	0.1	152.5	

B

Figure 1. Screenings of a DNA-encoded library (DELopen by WuXi AppTec) against GPX4 or a patient-derived variant of GPX4 (R152H). (A) Enrichment index of top hits from an affinity screening of 2.8 billion compounds in a DNA-encoded chemical library against negative control Ni-NTA magnetic beads and His-tagged GPX4^{WT} (U46C, two replicates) or GPX4^{R152H} (U46C-R152H) protein immobilized on the beads. Based on how hit compounds (DEL-A through DEL-K) enriched on WT vs R152H GPX4, screening hits are grouped as WT-selective (DEL-A and DEL-B), pan-GPX4 (DEL-C through DEL-G), or R152H-selective (DEL-H through DEL-K). (B) Structures of top screening hits that selectively enriched on GPX4^{R152H} (U46C-R152H). All screening hits are shown in Supplementary Figure S1.

After off-tag resynthesis, microscale thermophoresis (MST) binding analysis confirmed that Group 3 compounds bind to GPX4^{R152H} in vitro with higher binding affinities than they bind to GPX4^{WT}, while Group 1 compounds bind to GPX4^{WT} with higher affinity and Group 2 compounds exhibited similar affinities to WT and R152H GPX4 (Figures 2A,B and Supporting Information S2). Surface plasmon resonance (SPR) verified the affinity differences of the three groups of compounds, with most equilibrium dissociation constants (K_D) in line with those acquired from the MST binding assays (Supplementary Figure S3). Together, these biophysical data demonstrated the R152H-binding specificity of compounds in Group 3, as well as the WT-binding specificity of Group 1 compounds and pan-GPX4 binding affinity of Group 2 compounds, as predicted from the screening data.

It is noteworthy that regardless of WT or R152H selectivity, 8 of these top screening hits share benzisothiazolinone acetamide as a common scaffold, suggesting a GPX4 binding motif (Supplementary Figure S1B). Among these hits, as the exclusive R152H-selective binder, only DEL-I features an ethyl-pyridine side chain extending upward, while WT-selective binders DEL-A and DEL-B feature a biphenyl scaffold.

Variant-Specific Compounds Activate GPX4^{R152H} and Rescue Cells from Partial Loss of GPX4 Function. To investigate the R152H variant of GPX4 in a cellular context, we previously expressed human WT or R152H GPX4 in *Gpx4*-knockout cells.^{5,15,18–20} Using lysates of these cells, we

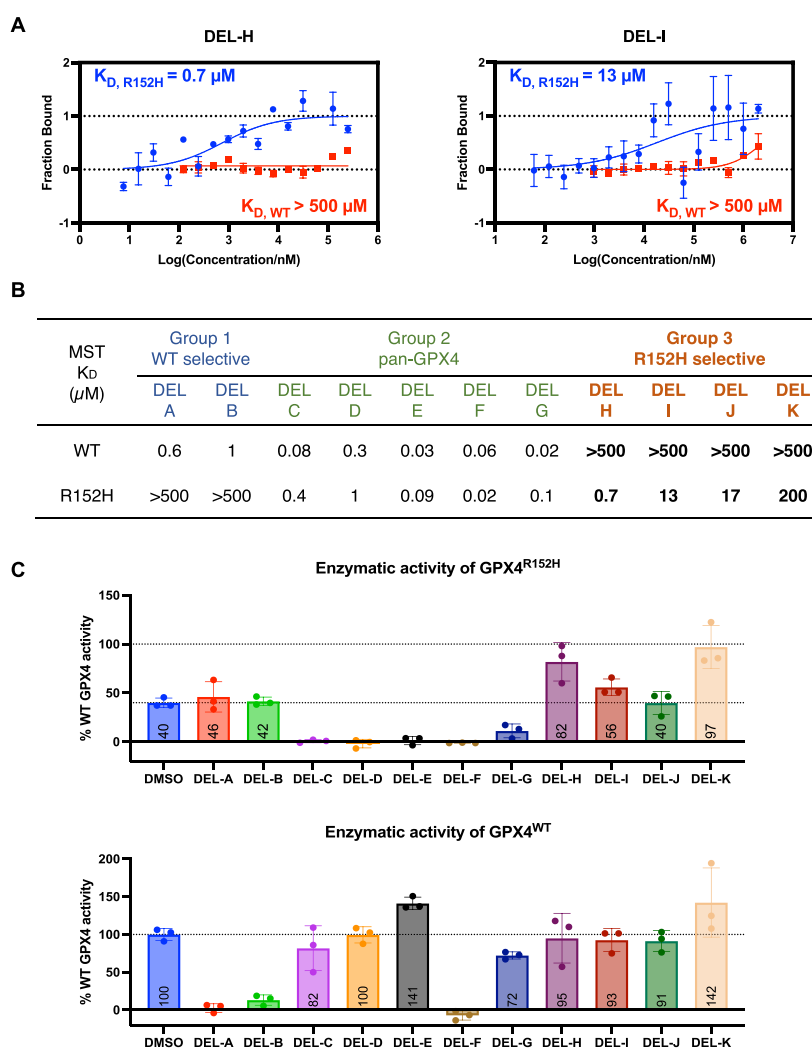


Figure 2. In vitro binding of screening hits to GPX4^{WT} and GPX4^{R152H}. (A) Binding affinities of DEL-H and DEL-I to GPX4^{WT} (U46C) and GPX4^{R152H} (U46C-R152H) as measured by microscale thermophoresis (MST). Data are plotted as means \pm s.d., $n = 2$ biologically independent samples. (B) Summary of binding affinities of screening hits to GPX4^{WT} (U46C) and GPX4^{R152H} (U46C-R152H) as measured by MST. (C) Enzyme activity of GPX4 in lysates of *Gpx4*-knockout Pfa-1 cells that were transfected to overexpress exogenous R152H (top panel) or WT (bottom panel) human GPX4 was measured in a NADPH-coupled assay after treatment with DMSO control or 200 μ M of each compound for 30 min. Activity was normalized and presented as percentage of WT GPX4 treated with DMSO. Data are plotted as means \pm s.d., $n = 3$ biologically independent samples.

examined the effect of DEL compounds on the enzymatic activity of transfected GPX4^{WT} or GPX4^{R152H} protein via measuring their ability to reduce a phospholipid hydroperoxide, a GPX4-specific substrate, in an NADPH-coupled assay, as reported previously.²¹ We found that the hit compounds DEL-H, DEL-I, and DEL-K in Group 3 selectively increased the enzymatic activity of cellular GPX4^{R152H} (40% GPX4^{WT}) to 82%, 56%, and 97% GPX4^{WT}, respectively, while they exhibited no significant effect on GPX4^{WT} (Figure 2C). In comparison, Group 1 compounds (WT-specific) selectively inhibited the enzymatic activity of cellular GPX4^{WT}, while they exhibited no significant effect on GPX4^{R152H}. In addition, Group 2 compounds (pan-GPX4) selectively inhibited the enzymatic activity of cellular GPX4^{R152H}, suggesting a protein binding mechanism different from that of the R152H-specific activating compounds in Group 3.

To further evaluate the therapeutic potency, we treated these cells with R152H-specific compounds and measured cellular viabilities: DEL-H, DEL-I, and DEL-K selectively increased cell number and viability of GPX4^{R152H}-expressing cells to 270%,

170%, and 240%, respectively, as compared to vehicle-treated control cells (Figures 3A and Supplementary S4A).

To validate these effects on the R152H variant in patient's cellular context, we previously developed fibroblasts from a patient homozygous for the R152H variant (RAG01, GPX4^{R152H/R152H}) and the patient's parent as an unaffected control with a heterozygous genotype⁵ (RAG02, GPX4^{R152H/WT}). The proof-of-concept treatments effective on engineered cells also consistently exhibited rescue effects on patient-derived fibroblast cells. DEL-H, DEL-I, and DEL-K selectively increased the viability of patient fibroblast RAG01 cells to 260%, 190%, and 230%, respectively, as compared to vehicle-treated control cells (Figures 3B and Supplementary S4B). It was noteworthy that the rescue effect was specific for RAG01, with no viability increase observed in the control RAG02 line. In comparison, Group 1 compounds (WT-specific) exhibited no rescue effect on patient-derived fibroblasts but suppressed the viabilities of the control RAG02 line (GPX4^{R152H/WT}), which is in line with their inhibitory effects on GPX4^{WT} enzymatic activity (Supplementary Figure S5).

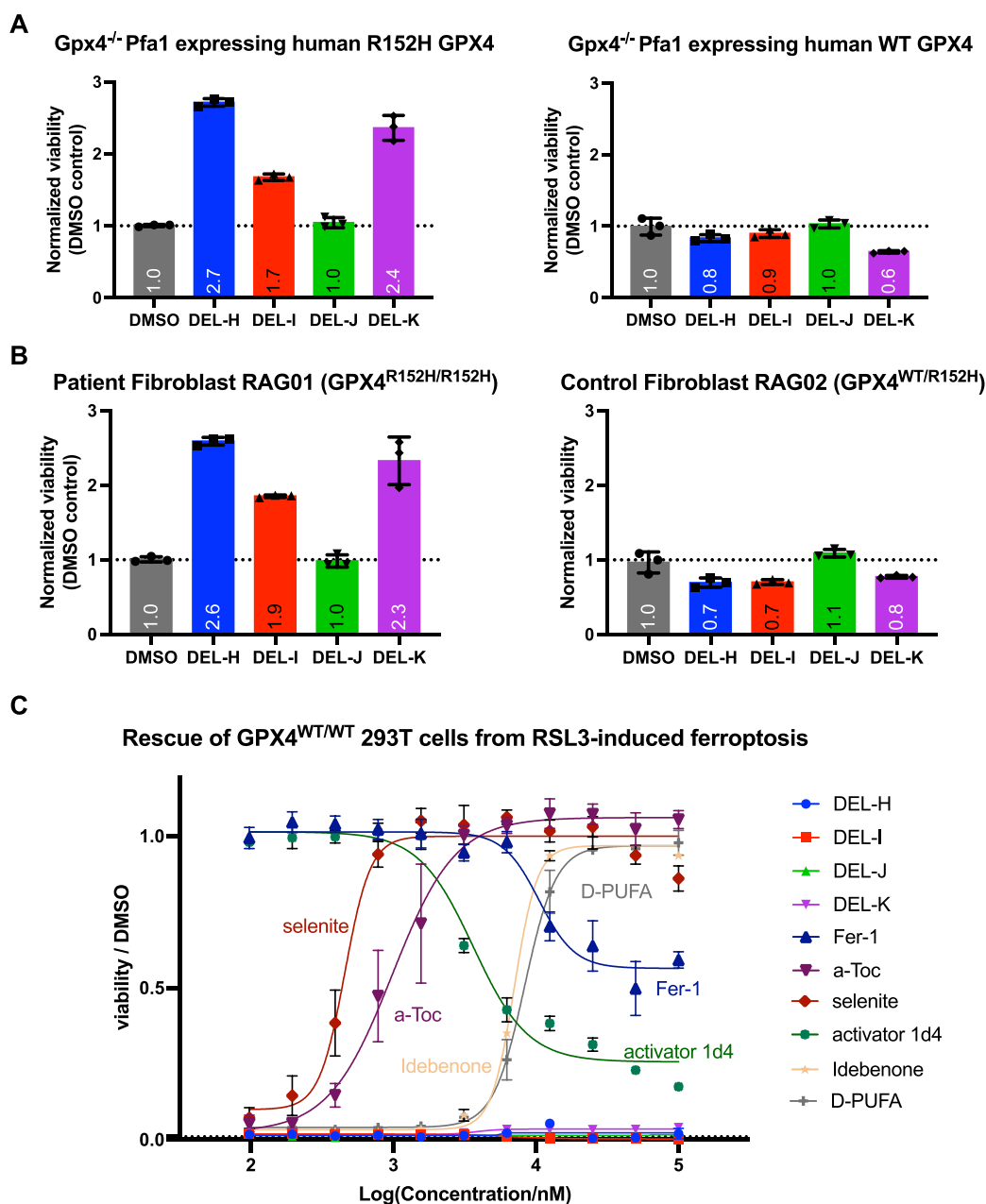


Figure 3. R152H-selective binders were tested as targeted proof-of-concept treatments. (A) Viability of *Gpx4*-knockout Pfa-1 cells transfected to overexpress exogenous R152H or WT human GPX4 was measured by CellTiter-Glo (CTG) luminescent cell viability assay, after treatment of DMSO control or DEL-H/I/J/K at serial diluted concentrations for 48 h. Viabilities of cells treated with compounds at EC₁₀₀ concentration on Pfa-1 cells that are transfected to express human GPX4^{R152H} (16 μ M of DEL-H, 63 μ M of DEL-I, 16 μ M of DEL-J, or 250 μ M of DEL-K) were normalized to DMSO control and plotted as means \pm SD, $n = 3$ biologically independent samples. (B) Viabilities of patient and control fibroblasts were measured by CTG luminescent cell viability assay, after treatment of DMSO control or DEL-H/I/J/K at serial diluted concentrations for 48 h. Viabilities of cells treated with compounds at EC₁₀₀ concentration on patient fibroblast (50 μ M of DEL-H, 100 μ M of DEL-I, 100 μ M of DEL-J, or 200 μ M of DEL-K) were normalized to DMSO control and plotted as means \pm SD, $n = 3$ biologically independent samples. (C) Viability of HEK-293T (GPX4^{WT/WT}) cells was measured by CTG luminescent cell viability assay after cotreatment of 0.2 μ M RSL3 and rescue compounds (DEL-H/I/J/K, Fer-1, α -Toc, selenite, GPX4 activator 1d4, idebenone, or D-PUFA) at serial diluted concentrations for 48 h. Viabilities were normalized to DMSO control and plotted as means \pm SD, $n = 3$ biologically independent samples.

Moreover, Group 2 compounds (pan-GPX4) reduced the viabilities of RAG01 and RAG02 fibroblasts. As both cell lines expressed GPX4^{R152H} protein, this is likely due to the inhibitory effects of Group 2 compounds on the GPX4^{R152H} enzymatic activity.

It is noteworthy that lipophilic antioxidants may also selectively boost the viability of patient-derived fibroblasts RAG01 via direct suppression of lipid peroxidation (for example,

α -tocopherol) or promotion of alternative antioxidation pathways (for example, Nrf2 activation by dimethyl fumarate).⁵ To test whether DEL hit compounds work through specific activation of GPX4^{R152H} to rescue RAG01 viability, we tested them in a commonly used human cell line HEK-293T, which only express GPX4^{WT}. We added the GPX4 inhibitor RSL3 to HEK-293T cells to induce ferroptosis⁴ and cotreated these ferroptotic cells with either DEL compounds or lipophilic

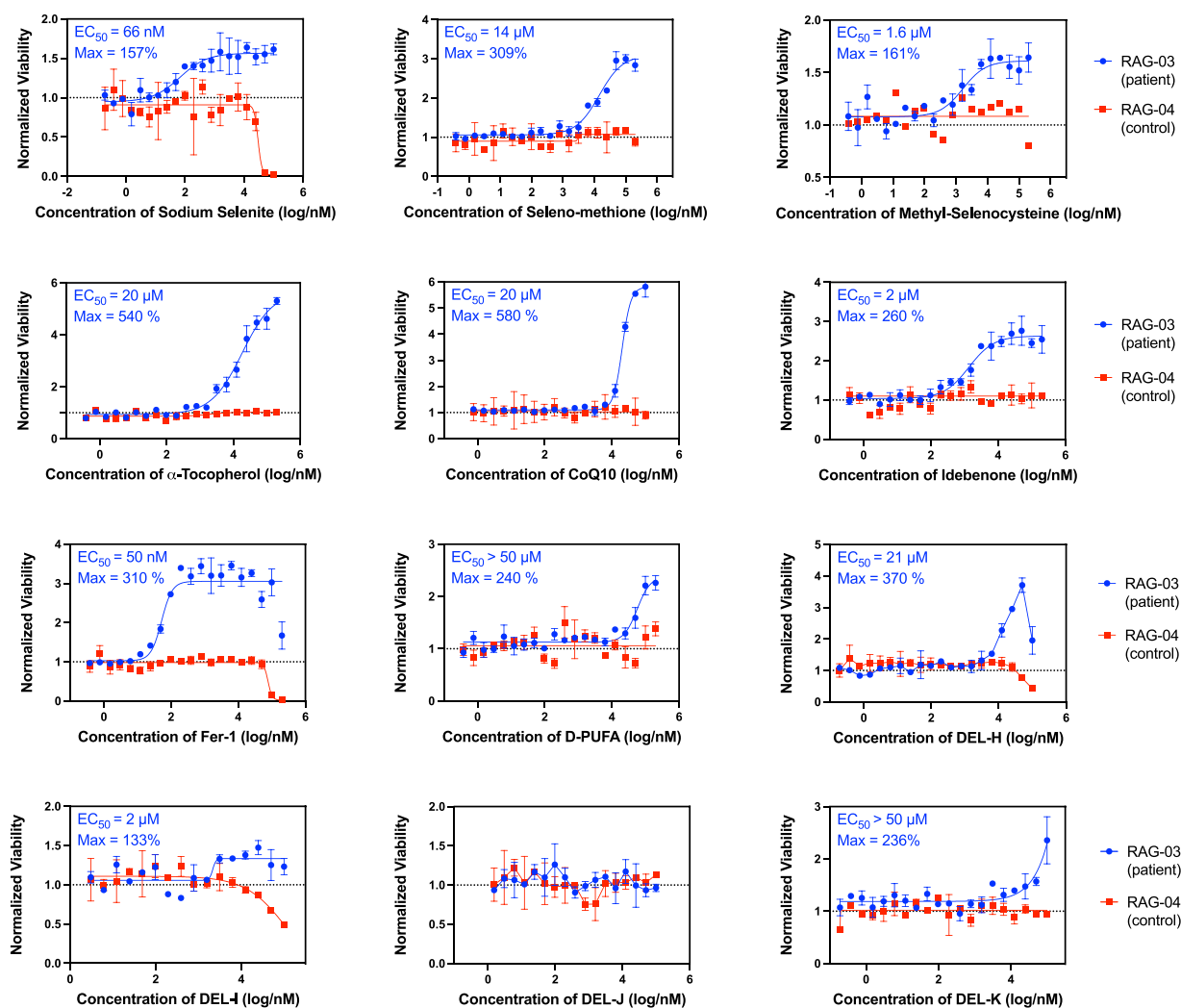


Figure 4. General and targeted proof-of-concept treatments on patient lymphoblasts. Supplements of sodium selenite (a), selenomethione (b), methyl-selenocysteine (c), α -tocopherol (d), CoQ10 (e), idebenone (f), Fer-1 (g), D-linoleic acid (h), DEL-H (i), DEL-I (j), DEL-J (k), and DEL-K (l) were tested as proof-of-concept treatments on the patient and control lymphoblast. α -Tocopherol was removed from the medium in advance, and lymphoblast cells were treated with proof-of-concept treatments on day 7 without α -tocopherol. The increase in cell number was monitored compared with cells treated with DMSO only. Data are plotted as means \pm s.d., $n = 3$ biologically independent samples.

antioxidants that had been shown to be effective previously to rescue RAG01 cells.⁵ As expected, lipophilic antioxidants rescued HEK-293T cells from RSL3-induced ferroptosis (Figure 3C). In comparison, DEL-H, DEL-I, and DEL-K exhibited no rescue effects in these ferroptotic cells, which only expressed GPX4^{WT}. This suggested that DEL-H, DEL-I, and DEL-K selectively rescued patient fibroblasts via specific activation of GPX4^{R152H}, rather than direct suppression of lipid peroxidation or promotion of alternative antioxidation pathways. Together, these data demonstrate the therapeutic potential of R152H-specific binders for SSMD patients with homozygous R152H variants of GPX4.

Effects of Proof-of-Concept Treatments are Similar in Patient Lymphoblasts. In addition to fibroblasts RAG01 and RAG02, B lymphocytes from the same patient and parent were also collected and subjected to Epstein–Barr virus (EBV) infection to induce continuous proliferation in vitro. We thus developed the human lymphoblast cell lines RAG03 (GPX4^{R152H/R152H}) and RAG04 (GPX4^{WT/R152H}). Different from fibroblast cells, which have a finite life span and limited passage number, lymphoblasts are immortalized and therefore

may serve as a more stable and consistent cell model to study the patient-derived variant and test the corresponding precision therapies.²²

To validate the relevance of lymphoblast cell models for drug discovery, we tested whether antioxidant treatments, which were effective at increasing the viability of patient-derived fibroblasts, also boosted the viability of the patient-derived lymphoblast RAG03. We first tested selenium supplementation (sodium selenite, selenomethione, or methylselenocysteine), which can boost expression of the R152H variant of the selenoprotein GPX4 protein to compensate for the partial loss of enzymatic function.²³ We found that sodium selenite, selenomethione, and methylselenocysteine could indeed increase the viability of the patient lymphoblast RAG03 line to 157%, 309%, and 161%, with an EC₅₀ (half maximal effective concentration) value of 66 nM, 14 μ M, and 1.6 μ M, respectively (Figure 4A–C). In addition, we evaluated the lipophilic antioxidants α -tocopherol, CoQ₁₀, and idebenone (a water-soluble analogue of CoQ₁₀), which can suppress lipid peroxidation in patient-derived cells²⁴ and found that they also boosted the viability of RAG03 cells to 540%, 580%, and 260%, with EC₅₀ values of 20 μ M, 20 μ M and 2 μ M,

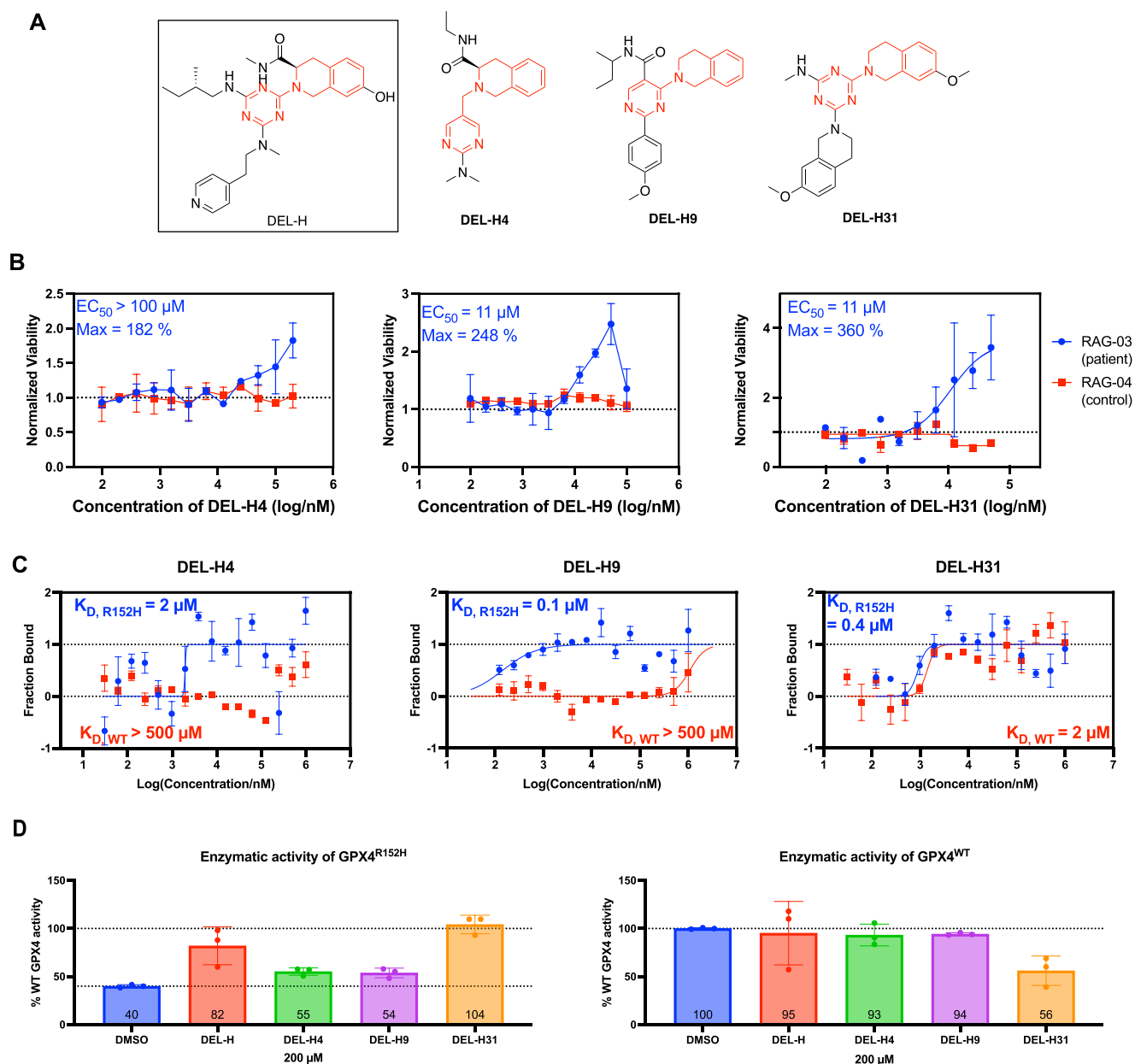


Figure 5. Structure and activity (SAR) study of DEL-H. (A) Structures of DEL-H and its analogues DEL-H4, DEL-H9, and DEL-H31. The common tetrahydroisoquinoline-like substructure is highlighted in red. (B) Treatments of DEL-H4, DEL-H9, and DEL-H31 were tested as proof-of-concept treatments on the patient and control lymphoblasts. α -Tocopherol was removed from the medium in advance, and lymphoblast cells were treated with proof-of-concept treatments on day 7 without α -tocopherol. The increase in cell number was monitored compared with cells treated with DMSO only. Data are plotted as means \pm s.d., $n = 2$ biologically independent samples. (C) Binding affinities of DEL-H4, DEL-H9, and DEL-H31 to GPX4^{WT} (U46C) and GPX4^{R152H} (U46C-R152H) as measured by MST. Data are plotted as means \pm s.d., $n = 2$ biologically independent samples. (D) Enzyme activity of GPX4 in lysates of *Gpx4*-knockout Pfa-1 cells that are transfected to overexpress exogenous R152H (left panel) or WT (right panel) human GPX4 was measured in a NADPH-coupled assay after treatment with DMSO control or 200 μ M of each compound for 30 min. Activity was normalized and presented as percentage of WT GPX4 treated with DMSO. Data are plotted as means \pm s.d., $n = 3$ biologically independent samples.

respectively (Figure 4D–F). Finally, we found that treatment with ferrostatin-1, a potent and selective inhibitor of ferroptosis,²⁵ and deuterium-reinforced linoleic acid (RT-001), a polyunsaturated fatty acid (PUFA) with deuterium at its bis-allylic site to inhibit lipid peroxidation,^{26–29} could substantially boost the viability of patient lymphoblast RAG03 cells to 310% and 240%, with an EC_{50} value of 50 nM and >50 μ M, respectively (Figure 4G,H). These pronounced rescue effects demonstrated the likely involvement of lipid peroxidation and ferroptosis in the compromised cell viability observed in the patient cells.

Moreover, Group 3 (R152H-specific) compounds DEL-H, DEL-I, and DEL-K also consistently exhibited rescue effects on patient-derived lymphoblasts (Figure 4I–L). Moving forward, we tested all additional compounds in the lymphoblasts, considering that they are immortalized with fewer limits on passage number, faster growing, and easier to culture as suspension cells.

Identification of Improved R152H-Selective Compounds from a Structure Activity Relationship Analysis of DEL-H. Although R152H-specific DEL screening hits boost the viabilities of the patient-derived lymphoblast RAG03 cell

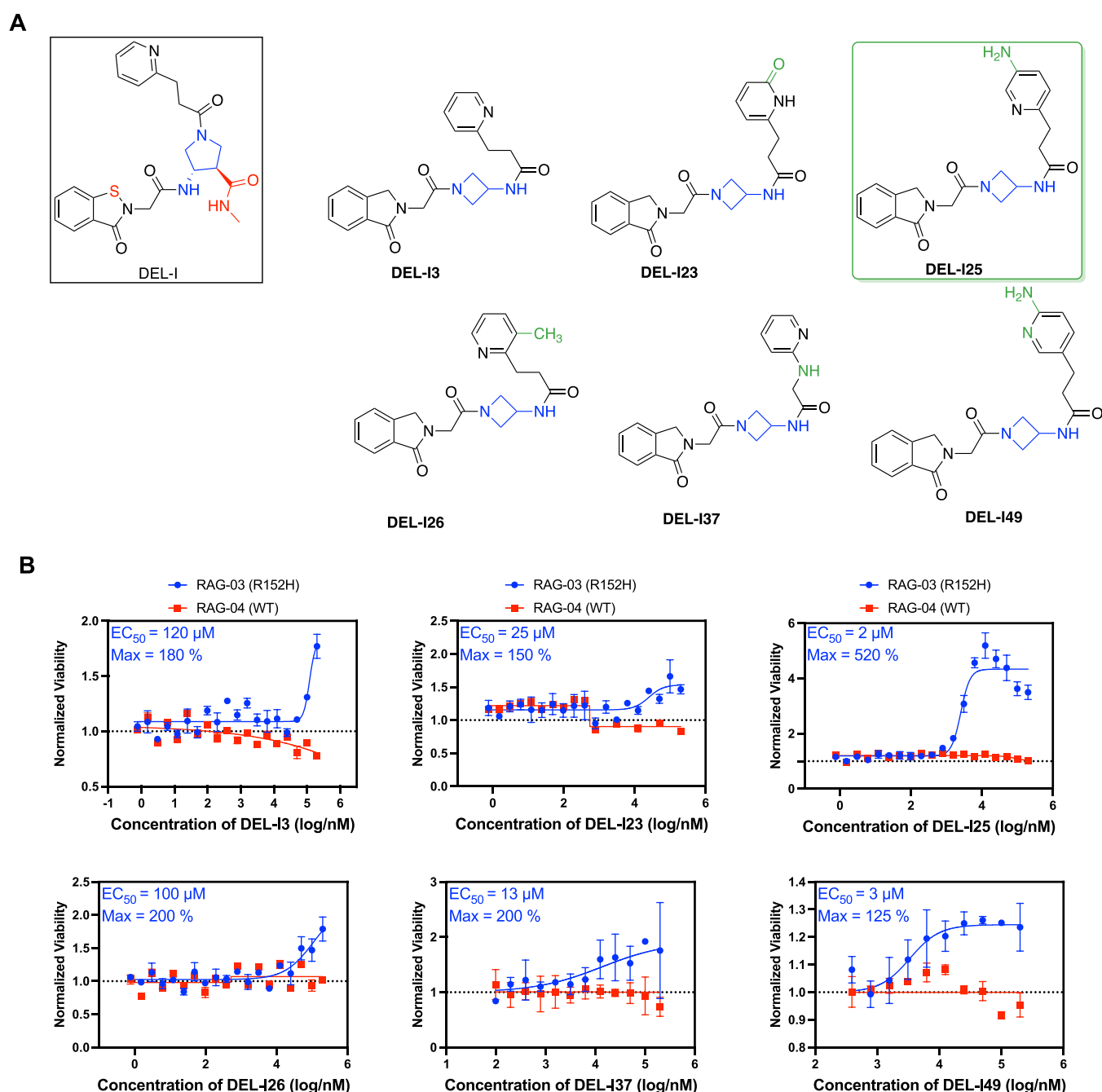


Figure 6. Optimized analogue of DEL-I exhibited improved potency to rescue patient lymphoblast cells. (A) Structures of DEL-I and its analogues DEL-I3, DEL-I23, DEL-I25, DEL-I26, DEL-I37, and DEL-I49. (B) Treatment of DEL-I3, DEL-I23, DEL-I25, DEL-I26, DEL-I37, and DEL-I49 were tested as proof-of-concept treatments on the patient and control lymphoblast. α -Tocopherol was removed from the medium in advance, and lymphoblast cells were treated with proof-of-concept treatments on day 7 without α -tocopherol. The increase in cell number was monitored compared with cells treated with DMSO only. Data are plotted as means \pm s.d., $n = 3$ biologically independent samples.

line, their rescue effects are less pronounced than the lipophilic antioxidants. DEL-H, DEL-I, and DEL-K boost the viability of RAG03 cells to 370%, 133%, and 236%, with EC₅₀ values of 21 μ M, 2 μ M, and >50 μ M. Aiming to develop R152H-specific binders with higher potency, we prioritized the structure–activity relationship (SAR) study of R152H-specific binders DEL-H and DEL-I, based on their higher binding affinity and selectivity toward GPX4^{R152H} in comparison with DEL-K, as observed in biophysical, biochemical, and cellular assays (Figures 2B,C and 3A).

Based on structural similarity, we tested a set of 16 analogues of DEL-H (DEL-H1 through DEL-H16, Supplementary Figures S6 and S7). We first tested them in RAG03 and RAG04 cells to screen for compounds that selectively increase the viability of patient-derived lymphoblasts (Supplementary Figures S8 and S9). We then conducted a counter screen in HEK-293T cells, as R152H-activating compounds should function specifically on GPX4^{R152H}, without a rescuing effect on RSL3-induced ferroptosis in cells exclusively expressing GPX4^{WT} (Supplementary Figure S10). Accordingly, we identified two analogues,

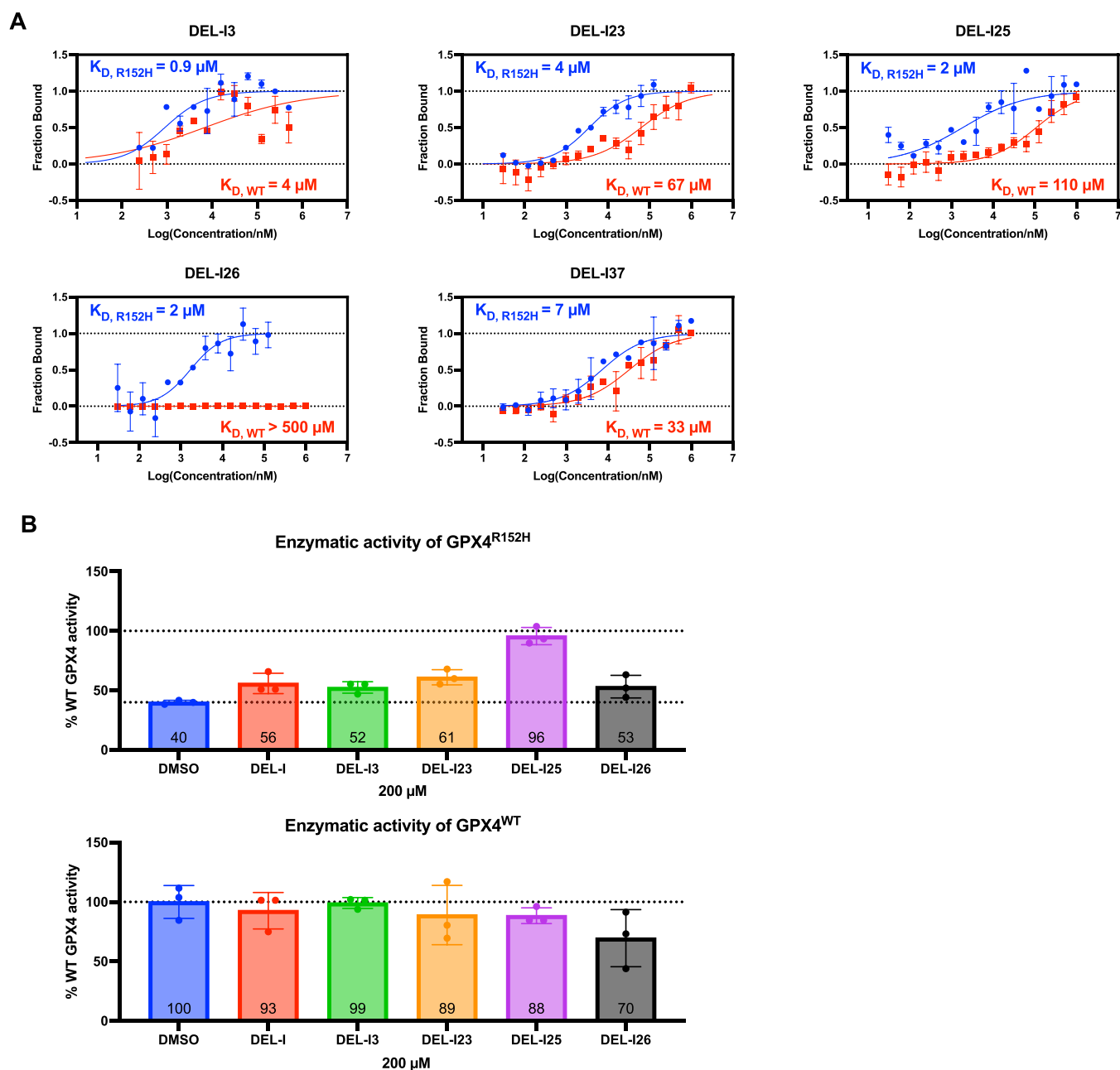


Figure 7. Optimized analogue of DEL-I binds to patient-derived variant of GPX4 with higher affinity and elevates its activity to a higher level, as compared to DEL-I. (A) Binding affinities of DEL-I3, DEL-I23, DEL-I25, DEL-I26, and DEL-I37 to GPX4^{WT} (U46C) and GPX4^{R152H} (U46C-R152H) as measured by MST. Data are plotted as means \pm s.d., $n = 2$ biologically independent samples. (B) Enzyme activity of GPX4 in lysates of *Gpx4*-knockout Pfa-1 cells that are transfected to overexpress exogenous R152H (top panel) or WT (bottom panel) human GPX4 was measured in a NADPH-coupled assay after treatment with DMSO control or 200 μ M of each compound for 30 min. Activity was normalized and presented as percentage of WT GPX4 treated with DMSO. Data are plotted as means \pm s.d., $n = 3$ biologically independent samples.

DEL-H4 and DEL-H9, that selectively increased the viability of RAG03 cells (Figure 5A,B).

Defining the common tetrahydroisoquinoline substructures shared by DEL-H, DEL-H4, and DEL-H9 as a core scaffold, we tested another set of 17 analogues of DEL-H (DEL-H17 through DEL-H33, Figures 5A and Supplementary S11, S12). With the cellular assays conducted in RAG03, RAG04, and HEK-293T cells, we identified one analogue, DEL-H31, that selectively rescued patient-derived lymphoblasts with potency slightly better than DEL-H (Figures 5A,B and Supplementary S10, S13, and S14). DEL-H31 can boost the viability of RAG03 cells to 360% with an EC_{50} value of 11 μ M.

MST-binding analysis demonstrated that DEL-H4, DEL-H9, and DEL-H31 bind to GPX4^{R152H} in vitro with higher binding affinities than GPX4^{WT}, while DEL-H9 and DEL-H31 exhibited lower K_D values (0.1 μ M and 0.4 μ M, respectively) than DEL-H ($K_D = 0.7 \mu$ M) for binding to GPX4^{R152H} (Figure 5C). This is in agreement with their lower EC_{50} values (both 11 μ M) than that of DEL-H ($EC_{50} = 21 \mu$ M) in the cellular assay.

While the GPX4 enzymatic activity assay demonstrated that DEL-H4, DEL-H9, and DEL-H31 selectively increased the enzymatic activity of cellular GPX4^{R152H}, DEL-H31 fully restored the enzymatic activity of GPX4^{R152H} to 104%

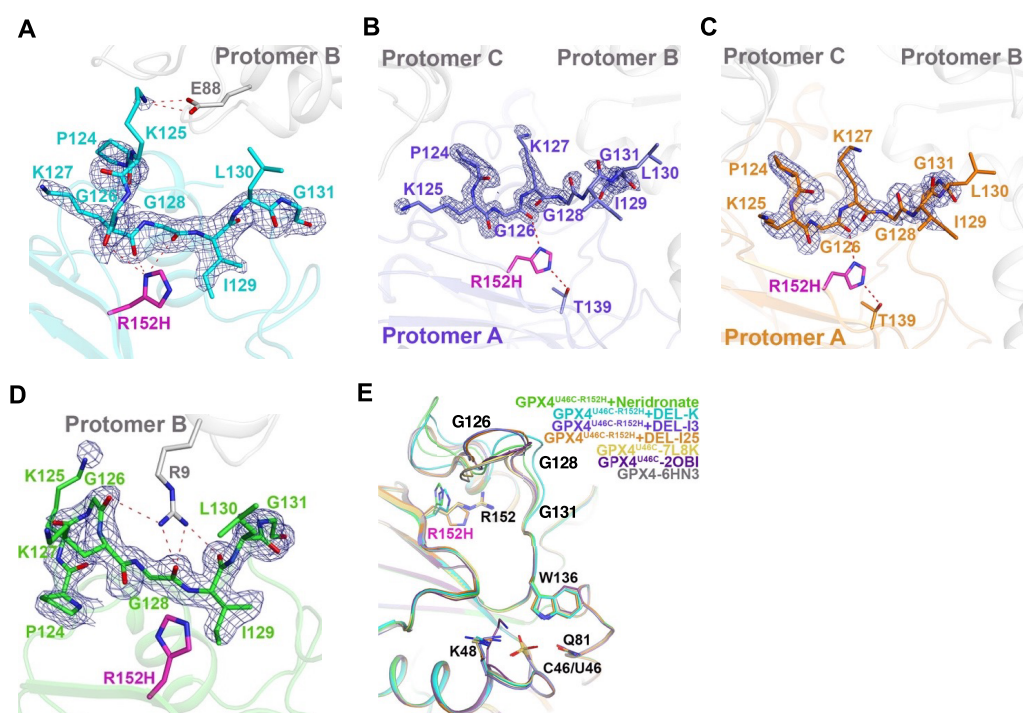


Figure 8. Crystal structure of the patient-derived R152H variant of GPX4 in the presence of DEL-K, DEL-I3, DEL-I25, and neridronate, where the disordered G-loop appeared to be conformationally stabilized. (A) Crystal structure of GPX4^{U46C-R152H} in the presence of 1 mM DEL-K. Two protomers of GPX4 (cyan and gray) are shown with cartoon representations. (B) Crystal structure of GPX4^{U46C-R152H} in the presence of 1 mM DEL-I3. Three protomers of GPX4 (purple for protomer A and gray for protomer B,C) are shown with cartoon representations. (C) Crystal structure of GPX4^{U46C-R152H} in the presence of 1 mM DEL-I25. Two protomers of GPX4 (orange and gray) are shown with cartoon representations. (D) Crystal structure of GPX4^{U46C-R152H} in the presence of 1 mM neridronate. Two protomers of GPX4 (green and gray) are shown with cartoon representations. For A–D, the mutated R152H residue in protomer A is shown in magenta. The side chain of part of the critical loop (G-loop, P124–N137) and its surrounding are shown as stick models. The 2Fo-Fc omit map contoured at 3σ is shown with density mesh. Hydrogen bonds are depicted as red dash lines. (E) Overlay of seven crystal structures of GPX4. Four crystal structures of GPX4^{U46C-R152H} shown in A–D are aligned with two crystal structures of GPX4^{U46C} (PDB codes: 7L8K and 2OBI) and one crystal structure of WT GPX4 without any mutations (PDB code: 6HN3). The side chain of part of the critical loop (G-loop, P124–N137) and its surrounding are shown as stick models. The active-site catalytic triad residues (W136, Q81, and C46/U46) are also shown as stick models.

GPX4^{WT}, which is more potent than DEL-H (82% GPX4^{WT}, Figure S5D).

Optimization of DEL-I Led to Discovery of Analogues with Improved Therapeutic Potency for R152H Patients.

When testing DEL-H analogues in RAG03 and RAG04 cells, we identified 10 compounds that selectively increase the viability of patient-derived RAG03 cells. But 7 out of the 10 compounds also rescued RSL3-induced ferroptosis in HEK-293T cells, suggesting they directly suppress lipid peroxidation or promote alternative antioxidation pathways (Supplementary Figure S10). Aiming to develop potent binders capable of the specific activation of GPX4^{R152H}, we focused on the optimization of DEL-I.

Based on structure similarity, we tested a set of 16 analogues of DEL-I (DEL-I1 through DEL-I16, Supplementary Figures S15 and S16). We first tested them in RAG03 and RAG04 cells, which was followed by a counter screen in HEK-293T cells. Accordingly, we identified one analogue, DEL-I3, which selectively rescued patient-derived lymphoblasts but with potency lower than DEL-I (Figures 6A,B and Supplementary S17–S19). DEL-I3 enhanced the viability of RAG03 cells to 180% with an EC₅₀ of 120 μM.

However, upon comparison of the chemical structure of DEL-I3 to that of the parent screening hit DEL-I, an *N*-methyl amide handle, which was used as linker to the DNA tag, was removed from the pyrrolidine ring (shown in red, Figure 6A).

Furthermore, a sulfur atom was substituted by a carbon to avoid potential covalent reactivity of the original ebselen-like structure with (seleno)cysteine residues³⁰ (shown in red, Figure 6A). The resulting compound DEL-I3, which has an additional rearrangement of the central diamine backbone (shown in blue, Figure 6A), is still active and able to rescue patient lymphocytes via interacting with GPX4^{R152H}. This suggested a core scaffold that is sufficient and essential for boosting GPX4^{R152H} activity. We therefore built around the structure of DEL-I3 with substitutions and modifications, which led us to test another set of 41 analogues of DEL-I and DEL-I3 (Supplementary Figures S20–S23).

With the multiplex cellular assays conducted in RAG03, RAG04, and HEK-293T cells, we identified five additional compounds (DEL-I23, DEL-I25, DEL-I26, DEL-I37, and DEL-I49) that selectively rescued patient-derived lymphoblasts with potency comparable to or better than that of DEL-I (Figures 6A,B and Supplementary S24–S27). These five compounds were indeed all close analogues of DEL-I3 with single modifications (shown in green, Figure 6A). We found that DEL-I23, DEL-I25, DEL-I26, DEL-I37, and DEL-I49 could boost the viability of patient lymphoblast RAG03 to 150%, 520%, 200%, 200%, and 125%, with an EC₅₀ value of 25 μM, 2 μM, 100 μM, 13 μM, and 3 μM, respectively. It is noteworthy that the top analogue DEL-I25 (properties shown in bold) featured substantial improvement over the original screening hit

DEL-I (max rescue = 133% with EC_{50} of 2 μ M). The maximal rescue effect of DEL-I25 on the patient lymphoblast was higher than the general antioxidant idebenone, ferroptosis inhibitor Fer-1 and D-linoleic acid, and any selenium supplementation at all tested concentrations. At the concentration of its EC_{100} (10 μ M), DEL-I25 is more therapeutically effective than general antioxidants α -tocopherol and CoQ₁₀ as well as all other tested proof-of-concept treatments.

MST binding analysis demonstrated that DEL-I3, DEL-I23, DEL-I25, DEL-I26, and DEL-I37 bind to GPX4^{R152H} in vitro with better binding affinities than GPX4^{WT}, with K_D values (0.9 μ M, 4 μ M, 2 μ M, 2 μ M, and 7 μ M, respectively) lower than DEL-I (K_D = 13 μ M) for binding to GPX4^{R152H} (Figure 7A). While the GPX4 enzymatic activity assay demonstrated that DEL-I3, DEL-I23, DEL-I25, and DEL-I26 selectively increased the enzymatic activity of cellular GPX4^{R152H}, notably DEL-I25 fully restored the enzymatic activity of GPX4^{R152H} to 96% of GPX4^{WT}, which is substantially more potent than DEL-I (56% of GPX4^{WT}, Figure 7B). From the structural aspect, DEL-I25 differs from DEL-I3 by the addition of an amino group ($-NH_2$) to make a 3-aminopyridine, a potential hydrogen bond donor and acceptor.

Crystal Structure Reveals That R152H-Specific Binders Can Stabilize the Disordered Critical Loop in GPX4^{R152H}.

Aiming to decipher the mechanism of the activation effects manifested by R152H-specific binders on GPX4^{R152H}, we determined three crystal structures of GPX4^{R152H} in the presence of R152H-specific binders (DEL-K, DEL-I3, and DEL-I25) and conducted structural analysis focusing on the loop between residue P124 and N137 (Figures 8 and Supplementary S28) as its structure is profoundly disrupted by the mutation and this is the exclusive structure difference between GPX4^{WT} and GPX4^{R152H} protein.⁵ This glycine-rich loop, the G-loop, contains three glycine residues. It is highly flexible in the crystal structures of GPX4 when it is exposed to a solvent. W136, which is essential for GPX4 enzymatic function as part of the catalytic triad at GPX4 active site,¹³ is on this critical G-loop (Figures 8E and Supplementary S28).

We first determined the crystal structure of GPX4^{R152H} in the presence of DEL-K (Figures 8A and Supplementary S28A). Although there was no electron density observed for DEL-K, the G-loop was moderately stabilized, as evidenced by clearly defined electron densities of the backbones of residues P124 and G131. This was in sharp contrast to the crystal structure of GPX4^{R152H} alone, where no electron density was observed for residues between P124 and G131.⁵ In this structure solved in the presence of DEL-K, the side chain of mutated residue H152 forms three weak hydrogen bonds with the backbone carbonyl groups of G126, K127, and G128, which may contribute to the stability of the G-loop. In addition, there is a weak salt bridge between K127 and E88 of a neighboring GPX4 (protomer B) protein in the crystal lattice, which might be an artifact of crystallization that also contributes to stabilization of the G-loop.

We also determined the crystal structure of GPX4^{R152H} in the presence of DEL-I3 (Figures 8B and Supplementary S28B). Despite the absence of any discernible electron density corresponding to DEL-I3, the G-loop was mostly ordered while being exposed to the solvent. More importantly, the G-loop adopted a conformation very similar to that in wild-type GPX4 (PDB id: 7L8K, Figures 8E and Supplementary S28E). In this structure solved in the presence of DEL-I3, the side chain of the mutated H152 formed two strong hydrogen bonds with the

backbone carbonyl group of G126 and the side chain of T139, which appears to be crucial in the stabilization of the G-loop. However, the electron density for the backbone of both I129 and L130 in the G-loop is weak compared to that in wild-type GPX4.

We then determined a crystal structure of GPX4^{R152H} in the presence of the top analogue DEL-I25 (Figures 8C and Supplementary S28C). While there was still no electron density observed for the small molecule, the G-loop was completely ordered with clearly defined backbone electron densities for all residues on the loop, albeit being exposed to a solvent. In this structure solved in the presence of DEL-I25, the G-loop conformation and H152-involved hydrogen bonding interactions are similar to those observed in the presence of DEL-I3. Furthermore, these stabilization effects of DEL-I3 and DEL-I25 are achieved without any observable interactions from neighboring GPX4 proteins, likely excluding contributions from crystallization artifact.

Inspired by the G-loop stabilization by hydrogen bonds and considering that arginine (R) has a longer side chain and is a better hydrogen bond donor and acceptor than histidine (H), we further tested and determined a crystal structure of GPX4^{R152H} in the presence of neridronate, a compound with a long alkyl chain and two phosphonate groups that are excellent hydrogen bond donors and acceptors (Figures 8D and Supplementary S28D). There was still no electron density for neridronate, and there were two GPX4 protomers in each unit cell of the crystal lattice. The G-loop in protomer B facing the solvent was mostly disordered (not shown), whereas the G-loop in protomer A was completely ordered because of four hydrogen bonds formed between R9 from protomer B with three backbone carbonyl groups of the G-loop in protomer A. Consequently, P124 adopted a *cis* conformation.

Overlay of the four crystal structures of GPX4^{R152H} determined in the presence of small molecules with the crystal structures of wild-type GPX4 (PDB id: 6HN3) revealed that the G-loop of GPX4^{R152H} in the presence of neridronate or DEL-K substantially deviates from the others, while the G-loop in the presence of DEL-I3 or DEL-I25 adopts a conformation similar to those in wild-type GPX4 (Figures 8E and Supplemental S28E).

A comparative analysis of *B*-factor values of each atom comprising the loop versus the entire protomer of each structure can provide additional insights into the flexibility of the G-loop among 6 crystal structures, as *B*-factor (also known as atomic displacement parameter) is an important criterion for assessing thermal motion of a protein in a given crystal lattice.³¹ Using this criterion, we first validated that the G-loop of GPX4 is more mobile than the rest of the protein, as the G-loop in all 6 structures has a higher average *B*-factor value than that of the entire protomer (Supplementary Table S1).

Furthermore, to compare G-loop stability across different structures, we quantified G-loop flexibility via dividing the average *B*-factor of the G-loop by that of the entire protomer for structures of GPX4^{R152H} that were obtained in the presence of DEL-I3 and DEL-I25 together with structures of wild-type GPX4^{U46C} (PDB id: 7L8K and 7L8Q) as these four structures have their loops facing the solvent and experience no observable intermolecular interactions from neighboring GPX4 macromolecules. The G-loop flexibility values for these structures are 2.55, 1.89, 1.54, and 1.50. This shows that DEL-I25 with a value of 1.89 is a better stabilizer of the G-loop as compared to DEL-I3 with a value of 2.55, which is consistent with biophysical and biochemical data (Supplementary Table S1).

In summary, based on crystal structures, DEL-K, DEL-I3, and DEL-I25 can stabilize the G-loop in GPX4^{R152H}, which contains residue W136 essential for GPX4 enzymatic activity and is disordered by the R152H mutation. Compared with DEL-K and DEL-I3, DEL-I25 can better stabilize the G-loop, which is in line with its capability to restore GPX4^{R152H} enzyme activity to a higher level and to rescue patient-derived lymphoblast cells to a substantially higher viability. Together, we validated a therapeutic strategy to apply variant-specific small-molecule binders to specifically restore activity of mutated pathological enzyme. The compounds that we developed, especially DEL-I25, feature the potential to be further developed into clinical treatments to benefit the SSMD patients with R152H point mutation.

DISCUSSION

In this study, we developed small molecules that can precisely bind to and restore the enzymatic activity of a patient-derived R152H variant of GPX4 to alleviate the pathological features caused by the loss-of-function mutation. Compared to general antioxidation treatments including α -tocopherol, which functions on downstream products of GPX4 and may interfere with other essential redox metabolism and signaling, our small molecules specifically target GPX4^{R152H}, the origin of the pathology, stabilize its structure, and restore its normal functions. A recent study found that the R152H mutation caused a reduction of cellular GPX4 catalytic efficiency due to an impaired coupling of GPX4 to mitochondria membrane with cardiolipin.³² Considering that alteration of the GPX4 subcellular localization was not observed in cells from patients with homozygous GPX4^{R152H}, the capability of our small molecules to rescue the viability of the patients' cells suggests they may reinstate the interaction of GPX4^{R152H} with cardiolipin and the sequential mitochondria membrane coupling, which is essential because mitochondria can act as initiators and amplifiers of ferroptosis especially for patients with homozygous GPX4^{R152H}.³³ Moreover, we devised a broadly applicable strategy to identify targeted small-molecule therapeutics for patients with missense mutations on crucial proteins, the pathology of which might not be curable by general antioxidants or other bulk supplements. Potential application of our strategy includes not only treatment of genetic disease with point mutations in specific proteins but also precision targeting of oncogenic mutations in cancers.

With SAR study on our screening hits DEL-H and DEL-I, we were able to improve their therapeutic potentials and resolve the cytotoxicity observed at high concentrations as the analogues became more tailored for GPX4^{R152H} (Supplementary Table S2). In our structural biology analysis, we found that the profound disruption of the G-loop (P124–N137) by the mutation is the exclusive structure difference between GPX4^{WT} and GPX4^{R152H} protein, and this loop contains W136, one of the catalytic triad of GPX4⁵. However, in the crystal structures of GPX4^{R152H} in the presence of our small molecules, we found that the G-loop is stabilized by multiple hydrogen bonds with G126, K127, and G128. This is in line with our SAR results, where we found that addition of hydrogen bond donor and acceptor functional groups onto DEL-I3 to generate analogues including DEL-I25 substantially improve the potency. Moreover, neridronate, a compound with a long alkyl chain and two phosphonate groups that are excellent hydrogen bond donors and acceptors, can also stabilize the G-loop. We envision that custom synthesis guided by our SAR results will further improve

their potency and pharmacokinetic properties including brain–blood barrier penetration, which could be another limitation of the lipophilic general antioxidation treatments.

When we profiled the binding affinities of DEL compounds to GPX4, the K_D values from MST and SPR assays were mostly in agreement. In general, we found that lower K_D values are mostly observed for compounds that feature higher potency in biochemical and cellular assays. In our SAR study, we identified compounds that can efficiently rescue cells from ferroptosis (e.g., DEL-H8, whose rescue effect on RSL3-induced ferroptosis in HEK293T cells is comparable to that of α -Tocopherol) as well as compounds that can bind to GPX4 with high affinity (e.g., DEL-H9, $K_D = 0.1 \mu\text{M}$). While these can be useful compounds for alternative purposes, for our aim in this study, we selected DEL-I25 as the top candidate, as it can selectively bind to GPX4^{R152H}, restore GPX4^{R152H} enzyme activity, and specifically rescue patient-derived lymphoblast cells.

It is noteworthy that PUFA-containing phospholipids can remodel cell membranes and promote cancer metastasis and resistance to chemotherapies, so aggressive cancer cells often exhibit elevated PUFA synthesis.^{8,9} But PUFAs are vulnerable to peroxidation, and GPX4 is the only enzyme capable of reducing PUFA-containing phospholipid hydroperoxide within cellular membranes.³⁴ Other glutathione peroxidases including GPX1 can only detoxify membrane phospholipid hydroperoxides after phospholipases release them into fatty acid hydroperoxides.³⁵ Therefore, these therapeutic-resistant cancers exhibit an elevated dependency on the GPX4 lipid peroxide repair pathway, and GPX4 inhibitors have been reported to be promising therapeutics to induce ferroptosis to drug-tolerant and metastatic cancers.^{7–9} We previously found that the destabilization of the G-loop in the GPX4 structure by the R152H mutation substantially impaired the enzymatic activity of GPX4⁵, while in this study we identified small molecules (e.g., DEL-25) that can stabilize the G-loop and restore the activity of GPX4. Considering that G-loop contains residue W136 which is essential for GPX4 enzymatic activity as part of the catalytic triad, these observations suggested that the stabilization of this G-loop is key to the catalytic activity of wild-type GPX4.

Since the side chains of two hydrophobic residues I129 and L130 curiously face the solvent in all reported crystal structures of WT GPX4 and GPX4^{U46C}, we hypothesize that they may play an important role in anchoring GPX4 to the membrane near the peroxidation site. Moreover, enzymes such as heme-dependent dioxygenases (i.e., tryptophan-2,3-dioxygenase, TDO) cleave O–O bonds in a highly hydrophobic, enclosed environment.³⁶ To achieve this, TDO has a glycine-rich loop near the heme, which acts as a gate that seals the active site as soon as Trp and O₂ enter the active site. If such a hydrophobic environment is also essential for efficient GPX4 activity, we wonder how the enzyme performs its function. GPX4 does not have a loop that could potentially act as a lid similar to that in TDO, which shields the active site during catalysis. Whether I129 and L130 likely play a role in creating a hydrophobic space for Sec46 to perform its function requires further investigation.

The importance of the G-loop in catalysis provides a strategy to inhibit GPX4 activity for targeting therapeutic resistant and metastatic cancers by destabilizing the G-loop. Indeed, our DEL screening hits in Group 1 (DEL-A and DEL-B, WT-GPX4-selective) and Group 2 (DEL-C through DEL-G, pan-GPX4) could all bind to WT GPX4 with high affinities and feature the potential to be developed into WT GPX4 inhibitors. Considering that a conformational change of the G-loop is the

exclusive structure difference between GPX4^{WT} and GPX4^{R152H}, small-molecule binders in Group 1 (WT-GPX4-selective) may be of interest for further investigation, as they may interact and destabilize the critical loop, inhibit WT GPX4 enzymatic activity, and therefore serve as leads for new cancer therapies.

METHODS

Cell Lines. HEK293T cells were obtained from ATCC and grown in DMEM with glutamine and sodium pyruvate (Corning 10-013) supplemented with 10% FBS and a 1% penicillin–streptomycin mix (Invitrogen). Human fibroblast cell lines RAG01 and RAG02 and human lymphoblast cell lines RAG03 and RAG04 were developed from a patient with homozygous R152H variant and his parent with heterozygous R152H variant. Preparation of RAG01 and RAG02 was described in the previous study.⁵ For lymphoblasts RAG04 and RAG04, B Lymphocytes from the patient and his parent were collected and subjected to EBV infection to induce their continuous proliferation in vitro. Infection of primary B cells was performed using wild-type EBV (2089) with a multiplicity of infection (MOI) of 0.1 overnight. This value of MOI provides the optimal conditions with respect to the number of emerging B blasts from EBV-infected primary naive B lymphocytes.³⁷ The next day, the cells were centrifuged (300 g at RT for 10 min) to remove unbound virus and were resuspended in fresh medium. Subsequently, infected cells were sorted and cell dividing index and cell cycle was calculated. RAG01, RAG02, RAG03, and RAG04 were grown in DMEM with glutamine and sodium pyruvate (Corning 10-013) supplemented with 15% FBS, 1% nonessential amino acids (Invitrogen), and 1% penicillin–streptomycin mix (Invitrogen). RAG01, RAG02, RAG03, and RAG04 cell lines are available for both commercial and academic use through CureGP-X4.org, a patient organization dedicated to finding a treatment for SSMD disease. Evaluation of the human fibroblast and lymphoblast cells, as part of the human subject protocol IRB-AAAS9249, was approved by the Rascal IRB of Columbia University.

The tamoxifen-inducible *Gpx4*-knockout Pfa1 murine cells over-expressing human WT or R152H exogenous GPX4 were used as described previously.^{5,15,18–20} These Pfa1 cells were grown in DMEM supplemented with 10% FBS, 1% glutamine, 1% penicillin–streptomycin mix, 750 μ g/mL neomycin, 1 μ M puromycin, and 1 μ M tamoxifen.

RAG01, RAG02, RAG03, RAG04, and *Gpx4*-knockout Pfa1 cells were supplemented with 10 μ M α -tocopherol (Sigma-Aldrich) if not otherwise stated. Cells were maintained in a humidified environment at 37 °C and 5% CO₂ in a tissue incubator.

Source of Compounds. WuXi AppTec, the provider of the DELopen library, conducted the off-tag resynthesis for desired GPX4 binders and provided resynthesized tag-free compounds DEL-A through DEL-K. Analogues of DEL-H and DEL-I were all commercially available compounds that were purchased from the chemical vendor Chemspace (DEL-H25, DEL-H28, DEL-H29, DEL-I1–DEL-I5, DEL-I7, and DEL-I17–DEL-I57, <https://chem-space.com>), Life Chemicals (DEL-H1–DEL-H3, DEL-H8–DEL-H12, DEL-H14, DEL-H15, and DEL-H16, <https://lifechemicals.com>), Enamine (DEL-H4–DEL-H7, DEL-H17–DEL-H24, DEL-H26, DEL-H27, DEL-H30–DEL-H33, DEL-I6, and DEL-I8–DEL-I11, <https://enamine.net>), and Otava (DEL-H13, DEL-H15, DEL-H16, and DEL-I12–DEL-I14, <https://www.otavachemicals.com>). This is summarized in Supplementary Table S3. RSL3 and Fer-1 were purchased from the chemical vendor Selleckchem (<https://www.selleckchem.com>). Sodium selenite, selenomethione, methylselenocysteine, α -tocopherol, CoQ₁₀, and idebenone were purchased from Sigma-Aldrich. D-PUFA (deuterium-substituted linoleic acid) was a generous gift of Mikhail S. Shchepinof from Retropro Inc. (Los Altos, CA, USA).

Expression and Purification of GPX4 Protein. Bacterial expression and purification of His-tagged-*c*-GPX4^{U46C_R152H} was described in a previous work⁵ and demonstrated here as well. With the previously generated and reported vector pOE30-His-tagged-*c*-GPX4^{U46C} as template,²⁸ the following mutagenesis primers were designed using the Agilent QuikChange Primer Design application:

R152H (F: 5'-CTG CGT GGT GAA GCA CTA CGG ACC CAT GG-3', R: 5'-CCA TGG GTC CGT AGT GCT TCA CCA CGC AG-3'). Primers were purchased from Integrated DNA Technologies. A site-directed mutagenesis kit (QuikChange II, Agilent 200521) was then used to acquire pOE30-His-tagged-*c*-GPX4^{U46C_R152H}. All mutations and the resulting plasmids were confirmed by sequencing at GENEWIZ.

Isolated colonies with the pOE30-His-tagged-*c*-GPX4^{U46C_R152H} or pOE30-His-tagged-*c*-GPX4^{U46C} plasmid were separately transferred to 8 mL of LB medium with 100 μ g/mL ampicillin, and the inoculated culture was incubated while being shaken (225 rpm) at 37 °C for 16 h. For each protein, 3 mL of the starter culture was added to 1 L of fresh LB medium with 100 μ g/mL ampicillin. The culture was incubated while being shaken at 37 °C and 225 rpm until the OD₆₀₀ reached 0.9. The temperature was then decreased to 15 °C. Cells were incubated with 1 mM isopropyl β -D-1-thiogalactopyranoside (IPTG) while being shaken at 15 °C and 225 rpm overnight. The next day, the bacteria were harvested by centrifugation at 4000g for 20 min at 4 °C and the pellet obtained was ready for purification or stored at –20 °C. The pellet was resuspended in 25 mL of chilled lysis buffer (100 mM Tris pH 8.0, 300 mM NaCl, 20 mM imidazole, 3 mM tris(2-carboxyethyl)phosphine hydrochloride (TCEP), and Roche protease inhibitor cocktail). The bacteria were lysed by sonication on ice for 6 min, and the lysate was centrifuged at 10000 rpm for 20 min at 4 °C to remove cell debris. The clarified lysate was incubated with Ni Sepharose 6 Fast Flow beads (GE Life Sciences) on a rotator at 4 °C for at least 1 h. The beads were washed with wash buffer (100 mM Tris at pH 8.0, 300 mM NaCl, 50 mM imidazole, and 3 mM TCEP) to remove nonspecific binding. The protein was eluted with 100 mM Tris at pH 8.0, 300 mM NaCl, 100 mM imidazole, and 3 mM TCEP. The protein was further purified using a gel filtration Superdex 200 column in FPLC buffer containing 100 mM Tris at pH 8.0, 300 mM NaCl, and 3 mM TCEP. The fractions containing GPX4 were pooled together and analyzed by sodium dodecyl sulfate–polyacrylamide gel electrophoresis (SDS–PAGE). GPX4 protein was then flash frozen with liquid nitrogen and stored at –80 °C before usage for binding assays and crystallography work.

DNA-Encoded Chemical Library (DELopen) Screening for GPX4 Binders. Access to DELopen, a DNA-encoded library of 2.8 billion compounds (as of the screening date, May 6th, 2020), was provided by WuXi AppTec. Access to this DELopen library for screening is free for academic laboratories. Top screening hit compounds (in our case DEL-A, DEL-B, DEL-C, ..., DEL-J, and DEL-K) can be purchased from WuXi AppTec for a fee.

We performed the screen against GPX4 using the DELopen kit and following the recommended protocol. To capture GPX4 protein onto beads for a pull-down binding affinity screening, we used His-tagged GPX4 and HisPur Ni-NTA magnetic beads (Thermo Scientific, #PI88831).

A bead capture test was first performed to confirm protein-bead immobilization efficiency. For each protein, 25 μ L of HisPur Ni-NTA magnetic beads were washed with 200 μ L of washing buffer (WB, provided by DELopen kit) three times, using a magnetic rack (DynaMag magnet, Invitrogen, #12321D) to separate beads from the supernatant. Beads were then suspended with 125 μ L of selection buffer (SB, provided by DELopen kit), with 25 μ L of suspended beads collected as Blank Beads control. Six microgram of His-tagged GPX4^{U46C_R152H} or GPX4^{U46C} protein was dissolved in 120 μ L of SB, with 1 μ g of each collected as Input control. The remaining 100 μ L of beads were pulled down before removal of the supernatant and mixed with the remaining 5 μ g of His-tagged protein in 100 μ L of SB. After incubation for 30 min at 25 °C with gentle rocking, beads were pulled down with the magnetic rack, with supernatant collected as flowthrough. Beads were then washed with 100 μ L of SB and pulled down with the magnetic rack, with supernatant collected as Wash. After resuspension in 100 μ L of SB, 50 μ L was collected as beads, while the other 50 μ L was incubated at 95 °C for 10 min. The heated beads were pulled down, and supernatant was collected as Heated Elution. Eventually, the remaining beads were resuspended in 50 μ L of SB and collected as heated beads. The samples collected above were analyzed

with gel electrophoresis and stained with Coomassie Blue before imaging to confirm protein-bead immobilization efficiency.

We used one DELopen kit. Since each kit provided four copies of library to screen for GPX4^{R152H} specific binders, two copies of the library were separately screened against beads with GPX4^{U46C} protein, one copy of the library was screened against beads with GPX4^{U46C-R152H} protein, and the fourth copy of the library was screened against the negative control beads with no protein immobilized. Such screening against different variants of protein may enable the identification of variant-specific binders. This is because we selected compounds selectively enriched on a specific variant of the protein.

Immobilization of His-tagged GPX4^{U46C-R152H} or GPX4^{U46C} was performed as described above for the beads capture test, using 20 μ L of beads and 5 μ g of protein as materials for each selection in each round. To include negative controls, protein buffer was used instead of protein to prepare vehicle control beads.

Three consecutive rounds of affinity selection were then performed. In each round of affinity selection, the beads for each corresponding condition were mixed with the library solution as dissolved in 100 μ L of SB. After an incubation for 1 h at 25 °C with gentle rocking, the beads were pulled down and washed with 200 μ L of SB buffer three times to remove unbound library molecules. The library molecules bound on immobilized GPX4 were released by incubating the SB-resuspended bead at 95 °C for 10 min, before pulling down the beads and collecting the supernatant. Part of the supernatant was set aside for future sequencing analysis, while the remaining supernatant was diluted to 100 μ L with SB and used as library solution for the next round of affinity selection. After the third selection, all heated supernatants were collected as an elution for future sequencing analysis.

The samples acquired from affinity selection were returned to WuXi AppTec, through which sequencing was performed to decode the DNA tags on library compounds to identify the top binders. WuXi AppTec then conducted the off-tag resynthesis for desired GPX4 binders, provided the resynthesized tag-free compounds for validation, and revealed the structure information for validated hits.

Microscale Thermophoresis. The binding affinities of compounds for His-tagged GPX4^{U46C-R152H} or GPX4^{U46C} were assayed using an MST-based Monolith NT.115 instrument (Nanotemper Technologies). His-tagged GPX4 was labeled with MST fluorescent dye using His-Tag Labeling Kit RED-tris-NTA second generation (MO-L018, Nanotemper Technologies) and following the manufacturer protocol: 100 nM GPX4 was incubated with 50 nM RED-tris-NTA dye in PBS-T buffer (1x PBS with 0.05% Tween 20) for 30 min at RT before centrifuging for 10 min at 4 °C and 15,000g to keep the supernatant only. The compounds were arrayed across a 2-fold dilution series in PBS-T buffer and separately mixed with the labeled GPX4 protein solution at a 1:1 ratio for a total of 20 μ L volume. Concentration of labeled GPX4 protein was constant in all mixtures. The mixtures were then loaded into standard capillaries (MO-K022, Nanotemper Technologies) and measured with MO.Control 2 Software (Nanotemper Technologies) using default settings on the Monolith NT.115 instrument, with 5 s of laser-on and 30 s of laser-off. All MST experiments were run in biological duplicates. Concentration range of individual compounds was determined by pilot experiments. The equilibrium dissociation constant (K_D) values were calculated by MO.AffinityAnalysis 3 Software (Nanotemper Technologies) on the Monolith NT.115 instrument, using duplicate ΔF_{norm} measurements to calculate the bound fraction at each concentration and fitting the data with a built-in K_D fit model. Figures were plotted with GraphPad Prism.

Surface Plasmon Resonance Binding Assays. The binding affinities of compounds for His-tagged GPX4^{U46C-R152H} or GPX4^{U46C} were also assayed using an SPR-based Biacore X100 instrument (Cytiva). His-tagged GPX4 was immobilized on a CMS5 sensor chip by using His Capture Kit (Cytiva, #2899S056) under standard condition at 25 °C with running buffer HBS-EP+ (10 mM HEPES, pH 7.4, 150 mM NaCl, 3 mM EDTA, and 0.05% v/v surfactant P-20). A reference flow cell was activated and blocked in the absence of GPX4. The GPX4 immobilization level was fixed at 1,000 response units, and then different concentrations of inhibitors were serially injected into the

channel to evaluate binding affinity. Between injections of inhibitors of different concentrations, regeneration of sensor chip was performed by washing with the regeneration buffer (20 mM glycine, pH 1.5) provided by the same His Capture Kit (Cytiva, #2899S056). The equilibrium dissociation constant (K_D) of the compounds was obtained by directly fitting SPR data with the built-in Biacore application using kinetic determination (X100 Evaluation Software, version 2.0.2).

Determination of GPX4-Specific Activity. We applied a NADPH-coupled cellular GPX4 enzymatic activity assay as previously reported.¹⁰ Oxidized glutathione, generated by GPX4 during reduction of its specific phospholipid hydroperoxide substrate, was reduced by glutathione reductase at the expense of NADPH, the decrease in the characteristic absorbance at 340 nm was monitored and quantified as GPX4 activity.

The GPX4-specific substrate phosphatidylcholine hydroperoxide (PCOOH) was prepared by enzymatic hydroperoxidation of phosphatidylcholine by soybean lipoxidase type IV: 22 mL of 0.2 M Tris-HCl, pH 8.8, containing 3 mM sodium deoxycholate and 0.3 mM phosphatidylcholine (Sigma-Aldrich) was incubated at RT, under continuous stirring, for 30 min with 0.7 mg of soybean lipoxidase type IV (Sigma-Aldrich). The mixture was loaded onto a Sep-Pak C18 cartridge (Waters-Millipore) washed with methanol and equilibrated with water. After washing with 10 vol of water, phosphatidylcholine hydroperoxides were eluted in 2 mL of methanol.

To measure the GPX4 activity, *Gpx4*-knockout Pfa1 murine cells overexpressing human WT or R152H exogenous GPX4 were harvested and lysed by LCW lysis buffer (0.5% TritonX-100, 0.5% sodium deoxycholate salt, 150 mM NaCl, 20 mM Tris-HCl pH 7.5, 10 mM EDTA, 30 mM Na-pyrophosphate, and complete protease inhibitor cocktail). The concentration of protein in the lysate was determined using the BCA assay kit using BSA as standards. To measure the effect of small molecules on GPX4 enzymatic activity, 3 μ L of 10 mM compounds or DMSO control were added to a 96-well plate first, before addition of 147 μ L of 1.5 μ g/ μ L cell lysate in the GPX4 activity assay buffer (0.1% Triton X-100, 100 mM Tris-HCl pH 7.4, 10 mM Na₃N, 5 mM EDTA, 0.6 IU/mL glutathione reductase, and 0.5 mM NADPH) and a sequential incubation at 37 °C for 20 min. PCOOH was then added to the mixture to initiate the GPX4 reaction. Absorbance of NADPH at 340 nm was determined kinetically at 1 min intervals over 20 min of time. GPX4 activity was calculated based on the consumption rate of NADPH during this kinetic process. Experiments using lysis buffer instead of cell lysate and controls without the addition of PCOOH were also done to measure the particular activity of GPX4 to reduce phospholipid hydroperoxides. Results were quantified by using GraphPad Prism 9.

Cellular Viability Assay. To monitor the viability of cells without α -tocopherol supplementation, cells that had been cultured in media with α -tocopherol supplementation were harvested with trypsin (if they are adherent cells), pelleted, and washed with PBS three times, counted by Vi-cell (Beckman), and then seeded into new cell culture flasks in media without α -tocopherol supplementation on day 1. On day 5, cells were harvested with trypsin and counted by Vi-cell before seeding back to the 384-well plates. For dose-response curves, 1,000 RAG01, RAG02, or Pfa-1 cells, or 10,000 cells of RAG03 or RAG04, were plated 36 μ L per well of a 384-well plate. Compounds were dissolved in DMSO, and a 2-fold dilution series was prepared. The compounds were then diluted 1:50 in media and 4 μ L was added to each well of the plates on day 5 as well. After 48 h of treatment, the viability of cells was measured using a 1:1 dilution of the CellTiter-Glo luminescent reagent (Promega G7573) with media, which was read on a Victor 5 plate reader after 10 min of shaking at RT. The intensity of luminescence was normalized to that of the DMSO control of each cell line. Results were quantified using GraphPad Prism 9.

Crystallization and Structure Determination. Protein sample of GPX4^{U46C-R152H} (4 mg mL⁻¹ GPX4^{U46C-R152H} in 20 mM Tris HCl, pH 8.0, 300 mM NaCl, 3 mM TCEP) in the presence of each activator was initially screened at the High-Throughput Crystallization Screening Center of the Hauptman-Woodward Medical Research Institute³⁸ (HWI) (<https://hwi.buffalo.edu/high-throughput-crystallization>

center/). The most promising crystal hits were subsequently reproduced using the oil micro batch method in a cold room at 4 °C.

Plate-like crystals of GPX4^{U46C-R152H} in the presence of 1 mM neridronate, DEL-K, DEL-I3, and DEL-I25 were grown using a crystallization reagent comprising 0.1 M 2-(*N*-morpholino)-ethanesulfonic acid (MES), pH 6, 0.1 M ammonium thiocyanate, and 20% (w/v) PEG 4000; 0.1 M MES, pH 6, 0.1 M lithium chloride, and 40% (w/v) PEG 8000; or 0.1 M Tris, pH 8, 0.1 M potassium thiocyanate, and 40% (w/v) PEG 8000. The last condition was used for crystallization of the enzyme with both DEL-I3 and DEL-I25. In all cases, the protein to crystallization reagent ratio was 2:1. All crystals were subsequently transferred into a similar crystallization reagent that was supplemented by 20% (v/v) ethylene glycol and flash-frozen in liquid nitrogen. Native data sets were collected on several crystals of GPX4^{U46C-R152H} in the presence of 1 mM Neridronate and DEL-I25 at the NE-CAT 24-ID-C beamline of Advanced Photon Source in Lemont, IL, while 24-ID-E was used for data collection on crystals of GPX4^{U46C-R152H} in the presence of 1 mM DEL-K and DEL-I3.

The best crystal of GPX4^{U46C-R152H} in the presence of neridronate, DEL-K, DEL-I3, and DEL-I25 diffracted X-ray at these two beamlines to resolutions 1.76, 1.74, 1.41, and 1.70 Å, respectively. The images were, respectively, processed and scaled in space groups *P*1, *P*₂₁₂₁, *P*₂₁₂₁, and *P*₂₁₂₁, using XDS³⁹ and Aimless.⁴⁰ The structure of each protein was determined by the molecular replacement method using the MOLREP⁴¹ program, and the crystal structure of GPX4^{U46C-R152H} (PDB id: 7L8L) was used as a search model for structure determination of four structures reported here. The models were rebuilt using programs XtalView⁴² and COOT⁴³ and refined by Phenix.⁴⁴ There are two protomers of GPX4^{U46C-R152H} in the asymmetric unit (ASU) of the crystal with space group *P*1 grown in the presence of neridronate, while the ASU of the other three structures (with space groups *P*₂₁₂₁, *P*₂₁₂₁, and *P*₂₁₂₁, respectively) contains one protomer. The crystallographic statistics are shown in Supplementary Table S4.

■ ASSOCIATED CONTENT

Data Availability Statement

Crystal structural coordinates were deposited in the RCSB, with accession codes PDB IDs: 8V1B, 8V1E, 8V1C, and 8V1D. Publicly available data sets used in this study are protein structures with PDB IDs: 2OBI, 6HN3, 7L8K, and 7L8Q. Source data are provided with this paper.

SI Supporting Information

The Supporting Information is available free of charge at <https://pubs.acs.org/doi/10.1021/acschembio.5c00158>.

(PDF)

(PDF)

(PDF)

(PDF)

Bead capture test and screenings hits of the DNA-encoded library screening, binding affinities of screening hits to GPX4, cellular viability assay data of screening hits, structures and cellular viability assay data of DEL-H analogues, structures and cellular viability assay data of DEL-H analogues, crystal structure of GPX4^{R152H} in the presence of selective activators, comparative analysis of average *B*-factors, summary of the key compounds and their properties, source of chemical compounds, and crystallography data collection and refinement statistics (PDF)

■ AUTHOR INFORMATION

Corresponding Author

Brent R. Stockwell – Department of Chemistry, Columbia University, New York, New York 10027, United States; Herbert Irving Comprehensive Cancer Center, Columbia

University, New York, New York 10032, United States; Department of Biological Sciences, Irving Institute for Cancer Dynamics, and Data Science Institute, Columbia University, New York, New York 10027, United States; Department of Pathology and Cell Biology and Columbia University Digestive and Liver Disease Research Center, Vagelos College of Physicians and Surgeons, Columbia University Irving Medical Center, New York, New York 10032, United States; orcid.org/0000-0002-3532-3868; Email: bstockwell@columbia.edu

Authors

Hengrui Liu – Department of Chemistry, Columbia University, New York, New York 10027, United States; orcid.org/0000-0002-5214-1572

Farhad Forouhar – Herbert Irving Comprehensive Cancer Center, Columbia University, New York, New York 10032, United States

Russell Saneto – Division of Pediatric Neurology, Department of Neurology, University of Washington, Seattle, Washington 98105, United States; Center for Integrative Brain Research, Seattle Children's Hospital, Seattle, Washington 98105, United States

Complete contact information is available at:

<https://pubs.acs.org/10.1021/acschembio.5c00158>

Author Contributions

B.R.S. and H.L. conceived and implemented the project. The planning and design of experiments was performed by H.L., F.F., and B.R.S. H.L. conducted protein purification, DEL screening, biophysical assays, biochemical assays, and cellular experiments. F.F. crystallized the proteins and collected diffraction data to solve the crystal structures. H.L., F.F., and B.R.S. wrote the manuscript.

Notes

The authors declare the following competing financial interest(s): B.R.S. is an inventor on patents and patent applications involving ferroptosis; co-founded and serves as a consultant to ProJenX, Inc. and Exarta Therapeutics; holds equity in Sonata Therapeutics; serves as a consultant to Weatherwax Biotechnologies Corporation and Akin Gump Strauss Hauer & Feld LLP. The remaining authors declare no competing interests.

Statistical Analyses: all replicate experiments, unless otherwise indicated, are biological replicates based on distinct samples.

■ ACKNOWLEDGMENTS

This study was supported by Columbia University Precision Medicine Initiative (to B.R.S.). We are grateful to the patient with the R152H variant and the patient's parent for providing their fibroblasts and lymphoblasts for this study. Crystallization screening at the National Crystallization Center at Hauptman-Woodward Medical Research Institute was supported through NIH grant R24GM141256. This work is based upon research conducted at the Northeastern Collaborative Access Team beamlines, which are funded by the National Institute of General Medical Sciences from the National Institutes of Health (P30 GM124165). The Eiger 16M detector on 24-ID-E is funded by a NIH-ORIP HEI grant (S10OD021527). This research used resources of the Advanced Photon Source, a U.S. Department of Energy (DOE) Office of Science User Facility operated for the DOE Office of Science by Argonne National Laboratory under

Contract no. DE-AC02-06CH11357. We are grateful to Mikhail S. Shchepinov from Retrotope Inc. for providing D-PUFA (deuterium-substituted linoleic acid). This study was supported by NIH grant numbers P30 GM124165, S10OD020056, S10OD030282, P30CA013696, 1P30DK132710.

REFERENCES

- (1) Kryukov, G. V.; et al. Characterization of mammalian selenoproteomes. *Science* **2003**, *300*, 1439–1443.
- (2) Ursini, F.; Maiorino, M.; Valente, M.; Ferri, L.; Gregolin, C. Purification from pig liver of a protein which protects liposomes and biomembranes from peroxidative degradation and exhibits glutathione peroxidase activity on phosphatidylcholine hydroperoxides. *Biochim. Biophys. Acta* **1982**, *710*, 197–211.
- (3) Stockwell, B. R.; et al. Ferroptosis: A Regulated Cell Death Nexus Linking Metabolism, Redox Biology, and Disease. *Cell* **2017**, *171*, 273–285.
- (4) Yang, W. S.; et al. Regulation of ferroptotic cancer cell death by GPX4. *Cell* **2014**, *156*, 317–331.
- (5) Liu, H.; et al. Characterization of a patient-derived variant of GPX4 for precision therapy. *Nat. Chem. Biol.* **2022**, *18*, 91–100.
- (6) Lerner, R. A.; Brenner, S. DNA-Encoded Compound Libraries as Open Source: A Powerful Pathway to New Drugs. *Angew. Chem., Int. Ed. Engl.* **2017**, *56*, 1164–1165.
- (7) Hangauer, M. J.; et al. Drug-tolerant persister cancer cells are vulnerable to GPX4 inhibition. *Nature* **2017**, *551*, 247–250.
- (8) Liu, H.; Schreiber, S. L.; Stockwell, B. R. Targeting Dependency on the GPX4 Lipid Peroxide Repair Pathway for Cancer Therapy. *Biochemistry* **2018**, *57*, 2059–2060.
- (9) Viswanathan, V. S.; et al. Dependency of a therapy-resistant state of cancer cells on a lipid peroxidase pathway. *Nature* **2017**, *547*, 453–457.
- (10) Janowski, R.; Scanu, S.; Niessing, D.; Madl, T. Crystal and solution structural studies of mouse phospholipid hydroperoxide glutathione peroxidase 4. *Acta Crystallogr., Sect. F: Struct. Biol. Commun.* **2016**, *72*, 743–749.
- (11) Li, C.; et al. Novel Allosteric Activators for Ferroptosis Regulator Glutathione Peroxidase 4. *J. Med. Chem.* **2019**, *62*, 266–275.
- (12) Sakamoto, K.; et al. Discovery of GPX4 inhibitory peptides from random peptide T7 phage display and subsequent structural analysis. *Biochem. Biophys. Res. Commun.* **2017**, *482*, 195–201.
- (13) Scheerer, P.; et al. Structural basis for catalytic activity and enzyme polymerization of phospholipid hydroperoxide glutathione peroxidase-4 (GPx4). *Biochemistry* **2007**, *46*, 9041–9049.
- (14) Borchert, A.; et al. Crystal structure and functional characterization of selenocysteine-containing glutathione peroxidase 4 suggests an alternative mechanism of peroxide reduction. *Biochim. Biophys. Acta, Mol. Cell Biol. Lipids* **2018**, *1863*, 1095–1107.
- (15) Ingold, I.; Berndt, C.; Schmitt, S.; Doll, S.; Poschmann, G.; Buday, K.; Roveri, A.; Peng, X.; Porto Freitas, F.; Seibt, T.; et al. Selenium Utilization by GPX4 Is Required to Prevent Hydroperoxide-Induced Ferroptosis. *Cell* **2018**, *172*, 409–422.
- (16) Yu, Y.; et al. Characterization and structural analysis of human selenium-dependent glutathione peroxidase 4 mutant expressed in *Escherichia coli*. *Free Radical Biol. Med.* **2014**, *71*, 332–338.
- (17) Moosmayer, D.; et al. Crystal structures of the selenoprotein glutathione peroxidase 4 in its apo form and in complex with the covalently bound inhibitor ML162. *Acta Crystallogr., Sect. D: Struct. Biol.* **2021**, *77*, 237–248.
- (18) Ingold, I.; et al. Expression of a Catalytically Inactive Mutant Form of Glutathione Peroxidase 4 (Gpx4) Confers a Dominant-negative Effect in Male Fertility. *J. Biol. Chem.* **2015**, *290*, 14668–14678.
- (19) Mannes, A. M.; Seiler, A.; Bosello, V.; Maiorino, M.; Conrad, M. Cysteine mutant of mammalian GPx4 rescues cell death induced by disruption of the wild-type selenoenzyme. *FASEB J.* **2011**, *25*, 2135–2144.
- (20) Seiler, A.; et al. Glutathione peroxidase 4 senses and translates oxidative stress into 12/15-lipoxygenase dependent- and AIF-mediated cell death. *Cell Metab.* **2008**, *8*, 237–248.
- (21) Roveri, A.; Maiorino, M.; Ursini, F. Enzymatic and immunological measurements of soluble and membrane-bound phospholipid-hydroperoxide glutathione peroxidase. *Methods Enzymol.* **1994**, *233*, 202–212.
- (22) Chuang, J. L.; Chuang, D. T. Diagnosis and Mutational Analysis of Maple Syrup Urine Disease Using Cell Cultures. In *Methods in Enzymology*; Harris, R. A.; Sokatch, J. R., Eds.; Academic Press, 2000; Vol. 324, pp 413–423.
- (23) Romanowska, M.; et al. Effects of selenium supplementation on expression of glutathione peroxidase isoforms in cultured human lung adenocarcinoma cell lines. *Lung Cancer* **2007**, *55*, 35–42.
- (24) Stockwell, B. R.; Jiang, X. The Chemistry and Biology of Ferroptosis. *Cell Chem. Biol.* **2020**, *27*, 365–375.
- (25) Dixon, S. J.; et al. Ferroptosis: an iron-dependent form of nonapoptotic cell death. *Cell* **2012**, *149*, 1060–1072.
- (26) Gaschler, M. M.; et al. FINO2 initiates ferroptosis through GPX4 inactivation and iron oxidation. *Nat. Chem. Biol.* **2018**, *14*, 507–515.
- (27) Hatami, A.; et al. Deuterium-reinforced linoleic acid lowers lipid peroxidation and mitigates cognitive impairment in the Q140 knock in mouse model of Huntington's disease. *FEBS J.* **2018**, *285*, 3002–3012.
- (28) Yang, W. S.; Kim, K. J.; Gaschler, M. M.; Patel, M.; Shchepinov, M. S.; Stockwell, B. R. Peroxidation of polyunsaturated fatty acids by lipoxygenases drives ferroptosis. *Proc. Natl. Acad. Sci. U.S.A.* **2016**, *113*, E4966–E4975.
- (29) Brenna, J. T.; et al. Plasma and Red Blood Cell Membrane Accretion and Pharmacokinetics of RT001 (bis-Allylic 11,11-D2-Linoleic Acid Ethyl Ester) during Long Term Dosing in Patients. *J. Pharm. Sci.* **2020**, *109*, 3496–3503.
- (30) Liu, H.; Iketani, S.; Zask, A.; Khanizeman, N.; Bednarova, E.; Forouhar, F.; Fowler, B.; Hong, S. J.; Mohri, H.; Nair, M. S.; et al. Development of optimized drug-like small molecule inhibitors of the SARS-CoV-2 3CL protease for treatment of COVID-19. *Nat. Commun.* **2022**, *13*, 1891.
- (31) Sun, Z.; Liu, Q.; Qu, G.; Feng, Y.; Reetz, M. T. Utility of B-Factors in Protein Science: Interpreting Rigidity, Flexibility, and Internal Motion and Engineering Thermostability. *Chem. Rev.* **2019**, *119*, 1626–1665.
- (32) Roveri, A.; et al. Cardiolipin drives the catalytic activity of GPX4 on membranes: Insights from the R152H mutant. *Redox Biol.* **2023**, *64*, 102806.
- (33) Stockwell, B. R. Ferroptosis turns 10: Emerging mechanisms, physiological functions, and therapeutic applications. *Cell* **2022**, *185*, 2401–2421.
- (34) Brigelius-Flohe, R.; Maiorino, M. Glutathione peroxidases. *Biochim. Biophys. Acta* **2013**, *1830*, 3289–3303.
- (35) Cheff, D. M.; et al. Development of an assay pipeline for the discovery of novel small molecule inhibitors of human glutathione peroxidases GPX1 and GPX4. *Redox Biol.* **2023**, *63*, 102719.
- (36) Forouhar, F.; et al. Molecular insights into substrate recognition and catalysis by tryptophan 2,3-dioxygenase. *Proc. Natl. Acad. Sci. U.S.A.* **2007**, *104*, 473–478.
- (37) Mrozek-Gorska, P.; et al. Epstein-Barr virus reprograms human B lymphocytes immediately in the prelatent phase of infection. *Proc. Natl. Acad. Sci. U.S.A.* **2019**, *116*, 16046–16055.
- (38) Budziszewski, G. R.; Snell, M. E.; Wright, T. R.; Lynch, M. L.; Bowman, S. E. J. High-Throughput Screening to Obtain Crystal Hits for Protein Crystallography. *J. Visualized Exp.* **2023**, *10*, 3791–65211.
- (39) Kabsch, W. Integration, scaling, space-group assignment and post-refinement. *Acta Crystallogr., Sect. D: Biol. Crystallogr.* **2010**, *66*, 133–144.
- (40) Evans, P. R.; Murshudov, G. N. How good are my data and what is the resolution? *Acta Crystallogr., Sect. D: Biol. Crystallogr.* **2013**, *69*, 1204–1214.
- (41) Vagin, A.; Teplyakov, A. Molecular replacement with MOLREP. *Acta Crystallogr., Sect. D: Biol. Crystallogr.* **2010**, *66*, 22–25.

- (42) McRee, D. E. XtalView/Xfit—A versatile program for manipulating atomic coordinates and electron density. *J. Struct. Biol.* **1999**, *125*, 156–165.
- (43) Emsley, P.; Lohkamp, B.; Scott, W. G.; Cowtan, K. Features and development of Coot. *Acta Crystallogr., Sect. D: Biol. Crystallogr.* **2010**, *66*, 486–501.
- (44) Adams, P. D.; et al. PHENIX: a comprehensive Python-based system for macromolecular structure solution. *Acta Crystallogr., Sect. D: Biol. Crystallogr.* **2010**, *66*, 213–221.